AIAA SciTech Forum
8-12 January 2024, Orlando, FL
AIAA SCITECH 2024 Forum
10.2514/6.2024-2825

Uncertainty in Wind Estimates, Part 2: H_∞ Filtering using Generalized Polynomial Chaos

Kenneth C. Gahan*, Jeremy W. Hopwood†, and Craig A. Woolsey‡
Virginia Polytechnic Institute and State University, Blacksburg, VA 24061

Indirect wind estimation onboard unmanned aerial systems (UASs) can be accomplished using existing air vehicle sensors along with a dynamic model of the UAS augmented with additional wind-related states. While many estimation approaches achieve desirable accuracy under the assumption of known system parameters, reducing the effect of parametric uncertainty on wind estimate precision is desirable and has not been thoroughly investigated. This paper describes the theory and process for using generalized polynomial chaos (gPC) to re-cast the dynamics of a system with non-deterministic parameters as a deterministic system. The concepts are applied to the problem of wind estimation and improving the precision of wind estimates over time due to known parametric uncertainties. In the multivariate case presented, a gPC H-infinity (H_∞) filter shows superiority over a nominal H_∞ filter in terms of variance in estimates due to model parametric uncertainty. The error due to parametric uncertainty, as characterized by the variance in estimates from the mean, is reduced by an average of ~25%.

I. Introduction

As explained in Part 1 of this two part series [1], wind estimation from air vehicle motion is useful for many reasons, including weather forecasting and air traffic management [2]. The ability to estimate wind indirectly (i.e. without specialized instrumentation) is of particular interest due to the increasing ubiquity of small unmanned aerial systems (UASs) [3] and the unobtrusive/low-cost nature of using operational sensors (e.g. air vehicle GPS, accelerometers, and gyroscopes). A common goal is to extract a mean component of the wind from higher frequency fluctuations (gusts or atmospheric turbulence). For example the United States' Automated Surface Observation System (ASOS), which provides crucial meteorological data to the National Weather Service (NWS), the Federal Aviation Administration (FAA), and the Department of Defense (DOD), reports averaged winds from higher frequency measurements [4].

Generally, estimation methods can be grouped into two major categories: model-based and model-free. Model-based estimation requires accurate aerodynamic and propulsive (aero-propulsive) models of the aircraft to generate state and wind estimates [5, 6]. Model-based methods are popular because they do not require direct measurement of the wind, such as with a pitot tube [7], and are thus readily applied to UASs. Present literature, however, often does not address the uncertainty in wind estimates due to uncertainties in the aircraft model.

Uncertainty refers to how imperfect knowledge is manifested in a system or process model [8]. Uncertainty quantification (UQ) is an estimation of the confidence in the output of that model [9]. Sources of uncertainty can generally be categorized as either *aleatory* uncertainty, which is inherent (irreducible) randomness in a system or process, or *epistemic* uncertainty, which is incomplete or inexact (reducible) encoding of the physical system or process to the model [10].

In Part 1, we presented the use of generalized Polynomial Chaos (gPC) to *analyze* the uncertainty in wind estimates due to aleatory uncertainty for any deterministic filtering method [1]. This work, however, presents a method of combining H-infinity (H_∞) filtering [11, 12] and gPC [13] to *reduce* the effect of aleatory uncertainty on wind estimates. Together, Parts 1 [1] and 2 demonstrate the utility and versatility of gPC in characterizing and mitigating uncertainty.

In Section II, we present the aircraft motion model upon which we develop the state estimator. In Section III we develop the methods for analyzing the uncertainty in wind estimates. Note that while much of Sections II and III are a review of Part 1, there are key differences which are necessary for the work presented here. The theory and steps involved in applying H_∞ filtering are given in Section IV. Section V presents an example using flight test data and multivariate uncertainty. In Section VI, we present the results and analysis. Lastly, in Section VII we present conclusions.

*PhD Candidate, Kevin T. Crofton Department of Aerospace and Ocean Engineering, AIAA Student Member
†PhD Candidate, Kevin T. Crofton Department of Aerospace and Ocean Engineering, AIAA Student Member
‡Professor, Kevin T. Crofton Department of Aerospace and Ocean Engineering, AIAA Associate Fellow

II. Aircraft Motion in Wind

A. Wind Field

Consider an aircraft in a wind velocity field, $\boldsymbol{W}$, that varies in space and time. At an instant of time, the wind velocity that would exist at the aircraft center of gravity (CG) if the aircraft were absent, the apparent wind, is

$$\boldsymbol{w}(t) = \boldsymbol{W}(\boldsymbol{X}(t), t) \tag{1}$$

where $\boldsymbol{X} = [X_N \;\; X_E \;\; X_D]^\mathsf{T}$ is the north-east-down position of the aircraft CG in an orthonormal Earth-fixed inertial reference frame $\mathcal{F}_\mathrm{I}$, defined by unit vectors $\{\boldsymbol{i}_1, \boldsymbol{i}_2, \boldsymbol{i}_3\}$. The total time derivative of the apparent wind is

$$\frac{\mathrm{d}\boldsymbol{w}}{\mathrm{dt}} = \frac{\partial \boldsymbol{W}(\boldsymbol{X}, t)}{\partial t} + \frac{\partial \boldsymbol{W}(\boldsymbol{X}, t)}{\partial \boldsymbol{X}} \frac{\mathrm{d}\boldsymbol{X}}{\mathrm{d}t} \tag{2}$$

Adopting the standard overdot notation for the total time derivative we have

$$\dot{\boldsymbol{w}} = \frac{\partial \boldsymbol{W}}{\partial t} + \frac{\partial \boldsymbol{W}}{\partial \boldsymbol{X}} \dot{\boldsymbol{X}} \tag{3}$$

Depending on the context, we adopt one of the following two assumptions about the dynamics of the wind field.

Assumption 1
(a) *The wind field evolves slowly compared to the aircraft velocity and is thus considered frozen, consistent with* Taylor*'s hypothesis [14], such that* $\frac{\partial \boldsymbol{W}}{\partial t} = \boldsymbol{0}$.
(b) *The variation of the wind field with position is negligible such that* $\frac{\partial \boldsymbol{W}}{\partial \boldsymbol{X}} = \boldsymbol{0}$.

The above assumption leads to the conclusion that $\dot{\boldsymbol{w}} = \boldsymbol{0}$ and the air relative angular velocity is equal to the vehicle angular velocity. This assumption, which is consistent with [2, 15], could be relaxed but it simplifies the results presented here.

Assumption 1 may seem incompatible with the motivating challenge of estimating variations in the wind velocity. However, the assumption of a uniform wind field does not impede the model-based filter from adjusting wind velocity estimates based on measurements.

Assumption 2 *The wind is a superposition of a bulk flow velocity (constant or slowly varying),* $\overline{\boldsymbol{w}}$*, and a higher frequency, finite-energy disturbance (gusts or turbulence),* $\delta\boldsymbol{w}$*, so that:*

$$\boldsymbol{w}(t) = \overline{\boldsymbol{w}}(t) + \boldsymbol{\delta w}(t) \tag{4}$$

Eq. (4) is known as a Reynolds decomposition [16] of the wind.

B. Nonlinear Equations for Fixed-Wing Aircraft Motion in Wind

Having discussed the dynamics of the wind field in Section II.A, we now briefly present the equations of motion for a fixed-wing aircraft in wind. The reader is directed to [17] and [18] for a full treatment of the derivation. We begin by defining the aircraft body reference frame, $\mathcal{F}_\mathrm{B}$, defined by orthonormal vectors $\{\boldsymbol{b}_1, \boldsymbol{b}_2, \boldsymbol{b}_3\}$ originating at the CG, where $\boldsymbol{b}_1$ points forward, $\boldsymbol{b}_2$ points out the right wing, and $\boldsymbol{b}_3$ completes the right-hand rule. The transformation from $\mathcal{F}_\mathrm{B}$ to $\mathcal{F}_\mathrm{I}$ is given by the rotation matrix

$$\boldsymbol{R}_{\mathrm{IB}}(\boldsymbol{\Theta}) = e^{[\boldsymbol{e}_3\times]\psi} e^{[\boldsymbol{e}_2\times]\theta} e^{[\boldsymbol{e}_1\times]\phi} \tag{5}$$

where $\boldsymbol{\Theta} = [\phi \;\; \theta \;\; \psi]^\mathsf{T}$ are the aircraft Euler angles, $\boldsymbol{e}_1 = [1\; 0\; 0]^\mathsf{T}$, etc., and $[(\cdot)\times]$ is the skew-symmetric cross product equivalent matrix satisfying $[\boldsymbol{a}\times]\boldsymbol{b} = \boldsymbol{a} \times \boldsymbol{b}$ for 3-vectors $\boldsymbol{a}$ and $\boldsymbol{b}$. Note that $\boldsymbol{R}_{\mathrm{BI}}(\boldsymbol{\Theta}) := \boldsymbol{R}_{\mathrm{IB}}^{-1}(\boldsymbol{\Theta}) = \boldsymbol{R}_{\mathrm{IB}}^{\mathsf{T}}(\boldsymbol{\Theta})$. The aircraft kinematics are given by

$$\dot{\boldsymbol{X}} = \boldsymbol{R}_{\mathrm{IB}}(\boldsymbol{\Theta})\boldsymbol{v} \tag{6}$$

$$\dot{\boldsymbol{R}}_{\mathrm{IB}}(\boldsymbol{\Theta}) = \boldsymbol{R}_{\mathrm{IB}}(\boldsymbol{\Theta})[\omega\times] \tag{7}$$

where $\boldsymbol{v} = [u \;\; v \;\; w]^\mathsf{T}$ is the velocity with respect to the inertial frame, given in the body frame, and $\boldsymbol{\omega} = [p \;\; q \;\; r]^\mathsf{T}$ is the angular velocity with respect to the inertial frame, expressed in the body frame. The matrix differential equation (7) holds independently of any attitude parameterization, but expanding the equation as written, with $\boldsymbol{R}_{\mathrm{IB}}$ as given in (5), yields the three conventional Euler angle rate equations:

$$\dot{\boldsymbol{\Theta}} = \boldsymbol{L}_{\mathrm{IB}}(\boldsymbol{\Theta})\boldsymbol{\omega} = \begin{bmatrix} 1 & \sin\phi\tan\theta & \cos\phi\tan\theta \\ 0 & \cos\phi & -\sin\phi \\ 0 & \sin\phi\sec\theta & \cos\phi\sec\theta \end{bmatrix} \begin{bmatrix} p \\ q \\ r \end{bmatrix} \tag{8}$$

As in [19] we make the assertion that the aerodynamic forces, $\boldsymbol{F}$, and moments, $\boldsymbol{M}$, depend on the velocity of the aircraft relative to the wind. For simplicity, we neglect any dependence of $\boldsymbol{F}$ and $\boldsymbol{M}$ on translational acceleration, such as the plunge acceleration ($\dot{w}$) dependence that often appears in fixed-wing flight dynamic models. Let

$$\boldsymbol{v}_{\mathrm{r}} = \boldsymbol{v} - \boldsymbol{R}_{\mathrm{BI}}(\boldsymbol{\Theta})\boldsymbol{w} \tag{9}$$

where $\boldsymbol{v}_{\mathrm{r}} = [u_{\mathrm{r}} \;\; v_{\mathrm{r}} \;\; w_{\mathrm{r}}]^{\mathsf{T}}$ is the velocity of the body's center of mass with respect to the wind, given in the body frame. Eq. (9) is known as the wind triangle. From Assumption 1, the air-relative angular velocity of the aircraft is equal to the total angular velocity, $\boldsymbol{\omega}$. Therefore, the aerodynamic force $\boldsymbol{F} = [X, Y, Z]^T$ and moment $\boldsymbol{M} = [L, M, N]^T$ have the general dependence

$$\boldsymbol{F} = \boldsymbol{F}(\boldsymbol{v}_{\mathrm{r}}, \boldsymbol{\omega}, \boldsymbol{u}), \quad \boldsymbol{M} = \boldsymbol{M}(\boldsymbol{v}_{\mathrm{r}}, \boldsymbol{\omega}, \boldsymbol{u}) \tag{10}$$

where the input $\boldsymbol{u} = [\delta_T \;\; \delta_a \;\; \delta_e \;\; \delta_{\mathrm{r}}]^{\mathsf{T}}$ comprises the throttle, aileron, elevator, and rudder control inputs. We use an aerodynamic model from [20] with non-dimensional coefficients of the form

$$C_X = X(\bar{q}S)^{-1} = C_{X_o} + C_{X_\alpha}\alpha + C_{X_{\alpha^2}}\alpha^2 + C_{X_{\delta_{\mathrm{e}}}}\delta_{\mathrm{e}} + C_T\delta_T \tag{11a}$$
$$C_Z = Z(\bar{q}S)^{-1} = C_{Z_o} + C_{Z_\alpha}\alpha + C_{Z_q}\hat{q} \tag{11b}$$
$$C_m = M(\bar{q}S\bar{c})^{-1} = C_{m_o} + C_{m_\alpha}\alpha + C_{m_q}\hat{q} + C_{m_{\delta_{\mathrm{e}}}}\delta_{\mathrm{e}} \tag{11c}$$
$$C_Y = Y(\bar{q}S)^{-1} = C_{Y_\beta}\beta + C_{Y_p}\hat{p} + C_{Y_r}\hat{r} + C_{Y_{\delta_{\mathrm{a}}}}\delta_{\mathrm{a}} + C_{Y_{\delta_{\mathrm{r}}}}\delta_{\mathrm{r}} \tag{11d}$$
$$C_l = L(\bar{q}Sb)^{-1} = C_{l_\beta}\beta + C_{l_p}\hat{p} + C_{l_{\delta_{\mathrm{a}}}}\delta_{\mathrm{a}} \tag{11e}$$
$$C_n = N(\bar{q}Sb)^{-1} = C_{n_\beta}\beta + C_{n_r}\hat{r} + C_{n_{\delta_{\mathrm{a}}}}\delta_{\mathrm{a}} + C_{n_{\delta_{\mathrm{r}}}}\delta_{\mathrm{r}} \tag{11f}$$

where the propulsion coefficient, C_T, is modeled using information from [21]. Here $\bar{q}$ is dynamic pressure, S is the wing planform area, $\bar{c}$ is mean aerodynamic chord, and b is wing span. Note that, in this section, the overhats ($\hat{}$) indicate nondimensional angular rates. In an abuse of notation, this symbol will later be used to denote estimates; the distinction will be clear from context. Here the angle-of-attack, α, and angle-of-sideslip, β, define the transformation between the body and wind-relative frames with

$$\alpha = \tan^{-1}\left(\frac{w_{\mathrm{r}}}{u_{\mathrm{r}}}\right) \qquad \text{and} \qquad \beta = \sin^{-1}\left(\frac{v_{\mathrm{r}}}{V_{\mathrm{r}}}\right) \tag{12}$$

where $V_{\mathrm{r}} = \|\boldsymbol{v}_{\mathrm{r}}\|$. Thus, the well established nonlinear equations of motion [17, 22], adapted for the assumed wind field, are

$$\dot{\boldsymbol{X}} = \boldsymbol{R}_{\mathrm{IB}}(\boldsymbol{\Theta})\boldsymbol{v}_{\mathrm{r}} + \boldsymbol{w} \tag{13a}$$
$$\dot{\boldsymbol{\Theta}} = \boldsymbol{L}_{\mathrm{IB}}(\boldsymbol{\Theta})\boldsymbol{\omega} \tag{13b}$$
$$\dot{\boldsymbol{v}}_{\mathrm{r}} = \boldsymbol{v}_{\mathrm{r}} \times \boldsymbol{\omega} + g\boldsymbol{R}_{\mathrm{BI}}(\boldsymbol{\Theta})\boldsymbol{e}_3 + \frac{1}{m}\boldsymbol{F}(\boldsymbol{v}_{\mathrm{r}}, \boldsymbol{\omega}, \boldsymbol{u}) \tag{13c}$$
$$\dot{\boldsymbol{\omega}} = \boldsymbol{I}^{-1}(\boldsymbol{I}\boldsymbol{\omega} \times \boldsymbol{\omega}) + \boldsymbol{I}^{-1}\boldsymbol{M}(\boldsymbol{v}_{\mathrm{r}}, \boldsymbol{\omega}, \boldsymbol{u}) \tag{13d}$$

where $\boldsymbol{I}$ is the aircraft moment of inertia tensor defined at the CG in $\mathcal{F}_B$. At last, we define the aircraft state and measurement equations

$$\dot{\boldsymbol{x}} = \boldsymbol{f}(\boldsymbol{x}, \boldsymbol{u}, \boldsymbol{w}) \tag{14a}$$
$$\boldsymbol{y} = \boldsymbol{h}(\boldsymbol{x}, \boldsymbol{u}) \tag{14b}$$

where the state, input, and wind vectors are

$$\boldsymbol{x} = \begin{bmatrix} \boldsymbol{X}^{\mathsf{T}} & \boldsymbol{\Theta}^{\mathsf{T}} & \boldsymbol{v}_{\mathrm{r}}^{\mathsf{T}} & \boldsymbol{\omega}^{\mathsf{T}} \end{bmatrix}^{\mathsf{T}}, \qquad \boldsymbol{u} = \begin{bmatrix} \delta_T & \delta_a & \delta_e & \delta_{\mathrm{r}} \end{bmatrix}^{\mathsf{T}}, \qquad \boldsymbol{w} = \begin{bmatrix} w_N & w_E & w_D \end{bmatrix}^{\mathsf{T}} \tag{15}$$

where the subscripts N, E, and D are north, east, and down, respectively. We will now present the linearized equations of motion for the aircraft in a wind field.

C. Linear, Small Perturbation Equations for Fixed-Wing Aircraft Motion in Wind

For the purpose of estimating the wind, it is assumed that the aircraft state of motion remains in the neighborhood of a nominal, equilibrium flight condition over a desired time or distance. This nominal flight condition is defined with regard to the *mean* wind field. The mean wind field is assumed to be steady and uniform. We let the subscript $\mathbf{eq} = \{(\boldsymbol{x}_\mathrm{e},\ \boldsymbol{u}_\mathrm{e},\ \boldsymbol{w}_\mathrm{e}) \mid \boldsymbol{x}_\mathrm{e} = \boldsymbol{u}_\mathrm{e} = \boldsymbol{w}_\mathrm{e} = \mathbf{0}\}$ denote the state and control variables and the mean wind velocity corresponding to a given, equilibrium flight condition (e.g., straight and level cruise in still air). Having defined a nominal, equilibrium state of motion, and assuming that the flight dynamic model is exact, any perturbations from the equilibrium flight condition that are not attributed to the initial state or control inputs can be ascribed to the wind disturbance.

To prepare for the formulation of a state estimator it is necessary to develop a linear time-invariant (LTI) model from the equations of motion given in Section II.B. Define

$$\boldsymbol{A} = \left.\frac{\partial \boldsymbol{f}}{\partial \boldsymbol{x}}\right|_{\mathbf{eq}} \qquad \boldsymbol{B} = \left.\frac{\partial \boldsymbol{f}}{\partial \boldsymbol{u}}\right|_{\mathbf{eq}} \qquad \boldsymbol{\Pi} = \left.\frac{\partial \boldsymbol{f}}{\partial \boldsymbol{w}}\right|_{\mathbf{eq}} \tag{16}$$

Linearizing the time-invariant system (13) about the equilibrium flight condition gives the LTI system

$$\Delta\dot{\boldsymbol{x}}(t) = \boldsymbol{A}\Delta\boldsymbol{x}(t) + \boldsymbol{B}\Delta\boldsymbol{u}(t) + \boldsymbol{\Pi}\Delta\boldsymbol{w}(t), \qquad \Delta\boldsymbol{x}(0) = \Delta\boldsymbol{x}_{\mathbf{0}} \tag{17a}$$

$$\boldsymbol{y}(t) = \boldsymbol{C}\Delta\boldsymbol{x}(t) + \boldsymbol{D}\Delta\boldsymbol{u}(t) + \boldsymbol{\Lambda}\boldsymbol{v}(t) \tag{17b}$$

where $\Delta\boldsymbol{x} \in \mathbb{R}^{n_x}$, $\Delta\boldsymbol{u} \in \mathbb{R}^{n_u}$, and $\Delta\boldsymbol{w} \in \mathbb{R}^{n_w}$ are perturbations from the equilibrium state, control, and wind vectors, and $\boldsymbol{v} \in \mathbb{R}^{n_v}$ is measurement noise. Note that while the position and heading variables in $\boldsymbol{x}_\mathrm{e}$ depend on time, they are ignorable coordinates in the dynamic equations and the resulting small perturbation model is LTI. For brevity, we will drop the Δ notation.

D. Low-pass Filter

As motivated in Section I, and detailed in [12, 23], we often wish to estimate the mean wind in the presence of disturbances. Thus, recalling from Assumption 3 that $\boldsymbol{w} = \overline{\boldsymbol{w}} + \boldsymbol{\delta w}$, we can design a low-pass filter to isolate the wind fluctuations of interest, given by the transfer function $\boldsymbol{H}_{\overline{\boldsymbol{w}}}(s)$ such that

$$\overline{\boldsymbol{w}}(s) := \boldsymbol{H}_{\overline{\boldsymbol{w}}}(s)\boldsymbol{w}(s) \tag{18}$$

Suppose Eq. (18) has the *state-space* realization

$$\dot{\boldsymbol{\zeta}}(t) = \boldsymbol{A}_{\overline{\boldsymbol{w}}}\boldsymbol{\zeta}(t) + \boldsymbol{B}_{\overline{\boldsymbol{w}}}\boldsymbol{w}(t) \tag{19a}$$

$$= \boldsymbol{A}_{\overline{\boldsymbol{w}}}\boldsymbol{\zeta}(t) + \boldsymbol{B}_{\overline{\boldsymbol{w}}}(\overline{\boldsymbol{w}}(t) + \boldsymbol{\delta w}(t)) \tag{19b}$$

$$\overline{\boldsymbol{w}}(t) = \boldsymbol{C}_{\overline{\boldsymbol{w}}}\boldsymbol{\zeta}(t) \tag{19c}$$

where $\boldsymbol{\zeta}$ is an intermediate state in the map from the wind input to the output of interest, $\overline{\boldsymbol{w}}$. We can now augment the system in Eq. (17) to obtain the system

$$\dot{\boldsymbol{x}}_A(t) = \underbrace{\begin{bmatrix} \boldsymbol{A} & \boldsymbol{\Pi}\boldsymbol{C}_{\overline{\boldsymbol{w}}} \\ \mathbf{0} & \boldsymbol{A}_{\overline{\boldsymbol{w}}} + \boldsymbol{B}_{\overline{\boldsymbol{w}}}\boldsymbol{C}_{\overline{\boldsymbol{w}}} \end{bmatrix}}_{\boldsymbol{A}_A} \boldsymbol{x}_A(t) + \underbrace{\begin{bmatrix} \boldsymbol{B} \\ \mathbf{0} \end{bmatrix}}_{\boldsymbol{B}_A} \boldsymbol{u}(t) + \underbrace{\begin{bmatrix} \boldsymbol{\Pi} \\ \boldsymbol{B}_{\overline{\boldsymbol{w}}} \end{bmatrix}}_{\boldsymbol{\Pi}_A} \boldsymbol{\delta w}(t), \qquad \boldsymbol{x}_A(0) = \boldsymbol{x}_{A_0} \tag{20a}$$

$$\boldsymbol{y}_A(t) = \underbrace{\begin{bmatrix} \boldsymbol{C} & \mathbf{0} \end{bmatrix}}_{\boldsymbol{C}_A} \boldsymbol{x}_A(t) + \boldsymbol{D}\boldsymbol{u}(t) + \boldsymbol{\Lambda}\boldsymbol{v}(t) \tag{20b}$$

where the augmented state is $\boldsymbol{x}_A = \begin{bmatrix}\boldsymbol{x}^\top & \boldsymbol{\zeta}^\top\end{bmatrix}^\top$. The exogenous inputs to Eq. (20) are grouped as $\boldsymbol{\eta} := \begin{bmatrix}\delta\boldsymbol{w}^\top & \boldsymbol{v}^\top\end{bmatrix}^\top$, so that

$$\dot{\boldsymbol{x}}_A(t) = \boldsymbol{A}_A\boldsymbol{x}_A(t) + \boldsymbol{B}_A\boldsymbol{u}(t) + \underbrace{\begin{bmatrix}\boldsymbol{\Pi} & \boldsymbol{0}\\ \boldsymbol{B}_{\overline{w}} & \boldsymbol{0}\end{bmatrix}}_{\boldsymbol{G}}\boldsymbol{\eta}(t) \tag{21a}$$

$$\boldsymbol{y}_A(t) = \boldsymbol{C}_A\boldsymbol{x}_A(t) + \boldsymbol{D}\boldsymbol{u}(t) + \underbrace{\begin{bmatrix}\boldsymbol{0} & \boldsymbol{\Lambda}\end{bmatrix}}_{\boldsymbol{F}}\boldsymbol{\eta}(t) \tag{21b}$$

$$\boldsymbol{z}(t) = \underbrace{\begin{bmatrix}\boldsymbol{L}_x & \boldsymbol{0}\\ \boldsymbol{0} & \boldsymbol{C}_{\overline{w}}\end{bmatrix}}_{\boldsymbol{L}}\boldsymbol{x}_A(t) \tag{21c}$$

where $\boldsymbol{z}$ are the outputs of interest when designing a filter that minimizes the worst-case effect of the exogenous disturbances, as will be shown presently.

III. Wind Estimation and Uncertainty

As described in Section II, a typical process for developing the linear aircraft model needed for wind estimation is to first postulate a nonlinear model structure, then identify the model parameters from experimentation, and lastly linearize about a desired condition. During the system identification process parametric uncertainty can largely be viewed as epistemic. That is, by gathering additional data or considering different model structures, with additional time and effort we could reduce the model uncertainty. Commonly used system identification processes [24, Ch. 6] aim at determining a model structure and model parameters for which the model prediction error is purely random. This purely random error is typically attributed to random disturbances and measurement noise in the output data used for model identification, but a direct consequence is a non-deterministic model in which the model parameters are described by probability distributions (e.g., mean and variance). For this reason, we consider the parameter uncertainty to be well described as aleatory.

This section describes the process of using gPC to reduce the effect of aleatory uncertainty in the aircraft model on wind estimates.

A. Mapping from Nonlinear Uncertainty to Linear Uncertainty

We first note that the nonlinear equations $\boldsymbol{f}$ can be separated into kinematic and dynamic equations, $\boldsymbol{f} = [\boldsymbol{f}_\mathrm{k}^\top \ \ \boldsymbol{f}_\mathrm{d}^\top]^\top$ respectively. In this work we seek to address the uncertainty in the dynamic equations, $\boldsymbol{f}_\mathrm{d}$, that arises from the aerodynamic parameters ($\boldsymbol{\vartheta} \in \mathbb{R}^m$) given in Table 5. The aerodynamic model (Eq. (11) is linear in its parameters. This is a common choice of model structure [24, Ch. 4]. Thus, the dynamic equations can be further separated into parts independent of and dependent upon $\boldsymbol{\vartheta}$:

$$\boldsymbol{f}_\mathrm{d}(\boldsymbol{x},\boldsymbol{u},\boldsymbol{\vartheta}) = \overline{\boldsymbol{f}}_\mathrm{d}(\boldsymbol{x},\boldsymbol{u}) + \sum_{i=1}^{m}\overline{\boldsymbol{g}}_i(\boldsymbol{x},\boldsymbol{u})\vartheta_i \tag{22}$$

We can similarly separate $\boldsymbol{A}$, $\boldsymbol{B}$, and $\boldsymbol{\Pi}$ into kinematic and dynamic components:

$$\boldsymbol{A} = \begin{bmatrix}\boldsymbol{A}_\mathrm{k}\\ \boldsymbol{A}_\mathrm{d}\end{bmatrix}, \quad \boldsymbol{B} = \begin{bmatrix}\boldsymbol{B}_k\\ \boldsymbol{B}_\mathrm{d}\end{bmatrix}, \quad \boldsymbol{\Pi} = \begin{bmatrix}\boldsymbol{\Pi}_\mathrm{k}\\ \boldsymbol{\Pi}_\mathrm{d}\end{bmatrix} \tag{23}$$

Then, from Eqs. (16) and (22), the elements of $\boldsymbol{A}_\mathrm{d}$ are

$$\mathrm{A}_{\mathrm{d}_{p,q}} = \left.\frac{\partial\overline{f}_{\mathrm{d}_p}}{\partial x_q}\right|_{\mathbf{eq}} + \sum_{i=1}^{m}\left.\frac{\partial\overline{g}_{i,p}}{\partial x_q}\right|_{\mathbf{eq}}\vartheta_i \tag{24}$$

The elements of $\boldsymbol{B}_\mathrm{d}$ and $\boldsymbol{\Pi}_\mathrm{d}$ are found similarly. Equation (24) gives an expression for how uncertainty in the nonlinear model parameters maps to uncertainty in the linear system. To simplify the presentation of gPC, in this work we make the following common assumption [25–27]:

Assumption 3 *The nonlinear model parameters are statistically independent [28].*

Under Assumption 3 we can use Eq. (24), along with knowledge of the nature of the uncertainty of the nonlinear model parameters, to determine the nature of the linear model uncertainties. Referring again to Table 5, the result of the system identification method used to find the nonlinear model parameters [20] is that $\vartheta_i \sim \mathcal{N}(\mu_i, \sigma_i^2)$. Thus, we can apply the *normal sum theorem* [28] to get

$$\mu(A_{\mathrm{d}_{p,q}}) = \left.\frac{\partial \bar{f}_{\mathrm{d}_p}}{\partial x_q}\right|_{\mathbf{eq}} + \sum_{i=1}^{m} \left.\frac{\partial \bar{g}_{i,p}}{\partial x_q}\right|_{\mathbf{eq}} \mu(\vartheta_i) \tag{25}$$

$$\sigma^2(A_{\mathrm{d}_{p,q}}) = \sum_{i=1}^{m} \left(\left.\frac{\partial \bar{g}_{i,p}}{\partial x_q}\right|_{\mathbf{eq}} \sigma(\vartheta_i) \right)^2 \tag{26}$$

We now have

$$\boldsymbol{A}(\boldsymbol{\xi}) = \begin{bmatrix} \boldsymbol{A}_{\mathrm{k}} \\ \boldsymbol{A}_{\mathrm{d}}(\boldsymbol{\xi}) \end{bmatrix} \tag{27}$$

where $\boldsymbol{\xi} \in \mathbb{R}^{n_\xi}$ is the vector of random parameters for the linear system. Following similar process we can find $\boldsymbol{B}(\boldsymbol{\xi})$ and $\boldsymbol{\Pi}(\boldsymbol{\xi})$.

B. Uncertain Augmented System

Consider the uncertain form of the augmented system equations

$$\dot{\boldsymbol{x}}_A(t, \boldsymbol{\xi}) = \boldsymbol{A}_A(\boldsymbol{\xi}) \boldsymbol{x}_A(t, \boldsymbol{\xi}) + \boldsymbol{B}_A(\boldsymbol{\xi}) \boldsymbol{u}(t) + \boldsymbol{G}\boldsymbol{\eta}(t) \tag{28a}$$

$$\boldsymbol{y}_A(t, \boldsymbol{\xi}) = \boldsymbol{C}_A \boldsymbol{x}_A(t, \boldsymbol{\xi}) + \boldsymbol{D}\boldsymbol{u}(t) + \boldsymbol{F}\boldsymbol{\eta}(t) \tag{28b}$$

$$\boldsymbol{z}(t, \boldsymbol{\xi}) = \boldsymbol{L}\boldsymbol{x}_A(t, \boldsymbol{\xi}) \tag{28c}$$

Note that, in general, $\boldsymbol{A}_A$ and $\boldsymbol{B}_A$ are functions of $\boldsymbol{\xi}$ due to uncertainty in $\boldsymbol{A}$ and $\boldsymbol{B}$ (the low-pass filter internal to $\boldsymbol{A}_A$ is deterministic). Thus $\boldsymbol{x}_A$, $\boldsymbol{y}_A$, and $\boldsymbol{z}$ are stochastic. The matrices $\boldsymbol{G}$, $\boldsymbol{C}_A$, $\boldsymbol{D}$, $\boldsymbol{F}$, and $\boldsymbol{L}$ are deterministic. Specifically, $\boldsymbol{C}_A$ and $\boldsymbol{D}$ are determined by available measurements, $\boldsymbol{L}$ defines desired estimates, and $\boldsymbol{G}$ and $\boldsymbol{F}$ are given by a known or assumed mapping of noise to the dynamics and measurements, respectively.

For these stochastic LTI equations we will use gPC to perform generalized polynomial chaos expansion (gPCE) which results in a deterministic system of equations. We will then use the resulting gPC system to characterize uncertainty in the wind estimates.

C. Generalized Polynomial Chaos

Let us define a tuple $\boldsymbol{j} = (j_1, \ldots, j_{n_\xi}) \in \mathbb{N}_0^{n_\xi}$* with $|\boldsymbol{j}| = j_1 + \cdots + j_{n_\xi}$ denoting the total degree of $\boldsymbol{j}$ [29]. We can construct multivariate gPC basis functions as products of univariate gPC polynomials according to the Weiner-Askey scheme [30]; i.e.,

$$\phi_{\boldsymbol{j}}(\boldsymbol{\xi}) = \phi_{j_1}(\xi_1) \ldots \phi_{j_{n_\xi}}(\xi_{n_\xi}), \quad 0 \le |\boldsymbol{j}| \le \infty \tag{29}$$

From [31], a second-order random process (i.e., finite variance) can be represented as a gPCE. Thus, for a function $\psi(\boldsymbol{\xi}) : \mathbb{R}^{n_\xi} \to \mathbb{R}$

$$\psi(\boldsymbol{\xi}) = \sum_{|\boldsymbol{j}|=0}^{\infty} \psi_{\boldsymbol{j}} \phi_{\boldsymbol{j}}(\boldsymbol{\xi}) \tag{30}$$

where $\{\psi_{\boldsymbol{j}}\}$ are the expansion coefficients. This expansion converges in the $\mathcal{L}_2$ sense [31, 32]. Fundamental to the concept of gPCE is the orthogonality of basis functions with respect to the distribution $\varphi(\boldsymbol{\xi})$ of $\boldsymbol{\xi}$, where $\varphi(\boldsymbol{\xi}) = \Pi_{k=1}^{n_\xi} \varphi_k(\xi_k)$.

*$\mathbb{N}_0$ are the natural numbers including 0

That is

$$\left\langle \phi_{\boldsymbol{j}}(\boldsymbol{\xi}), \phi_{\boldsymbol{k}}(\boldsymbol{\xi}) \right\rangle := \int_{\boldsymbol{\Omega}} \phi_{\boldsymbol{j}}(\boldsymbol{\xi}) \phi_{\boldsymbol{k}}(\boldsymbol{\xi}) \varphi(\boldsymbol{\xi}) \mathrm{d}\boldsymbol{\xi} \tag{31a}$$

$$= \mathbb{E}_{\xi}\{\phi_{\boldsymbol{j}}(\boldsymbol{\xi}) \phi_{\boldsymbol{k}}(\boldsymbol{\xi})\} \tag{31b}$$

$$= \begin{cases} \left\langle \phi_{\boldsymbol{j}}(\boldsymbol{\xi}), \phi_{\boldsymbol{j}}(\boldsymbol{\xi}) \right\rangle, & \text{if } \boldsymbol{j} = \boldsymbol{k} \\ 0, & \text{if } \boldsymbol{j} \neq \boldsymbol{k} \end{cases} \tag{31c}$$

where $\boldsymbol{\Omega}$ is the support of $\varphi(\boldsymbol{\xi})$ given by $\boldsymbol{\Omega} = \Omega_1 \times \cdots \times \Omega_{n_\xi}$ [30]. In practice it is not feasible to perform an exact gPCE, as this requires an infinite number of basis functions. Instead the gPCE is truncated to some suitably high order such that the total degree $|\boldsymbol{j}| \leq p$:

$$\psi(\boldsymbol{\xi}) \approx \sum_{|\boldsymbol{j}|=0}^{p} \psi_{\boldsymbol{j}} \phi_{\boldsymbol{j}}(\boldsymbol{\xi}) =: \tilde{\psi}(\boldsymbol{\xi}) \tag{32}$$

where the number of expansion factors, N_p, is given by

$$N_p = \binom{n_\xi + p}{p} := \frac{(n_\xi + p)!}{p!(n_\xi + p - p)!} = \frac{(n_\xi + p)!}{n_\xi! p!} \tag{33}$$

where p is the polynomial order. For convenient manipulation of the multi-index $\boldsymbol{j}$, the graded lexicographic order (GLO) is often used [29], where $\boldsymbol{k} > \boldsymbol{j}$ if $|\boldsymbol{k}| > |\boldsymbol{j}|$ or if $|\boldsymbol{k}| = |\boldsymbol{j}|$ and the first nonzero entry in $\boldsymbol{k} - \boldsymbol{j}$ is positive. Table 1 depicts the resulting ordering for a 3-tuple, as well as the associated single-index j'. The orthogonality property expressed in Eq. (31) ensures that $\tilde{\psi}(\boldsymbol{\xi})$ is the minimum error (ϵ) representation of $\psi(\boldsymbol{\xi})$ with respect to the Euclidean norm on the space spanned by the truncated basis functions [33]. This is known as a Galerkin projection [33]. Figure 1 depicts this concept for a two-term gPCE in a single uncertain variable.

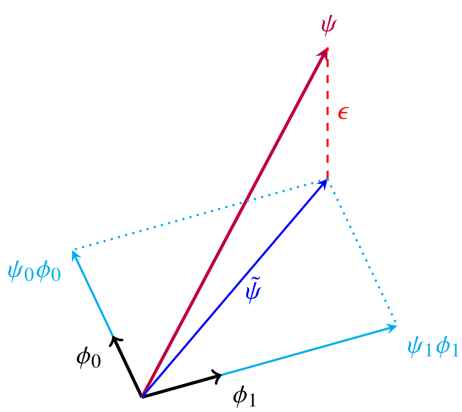

Fig. 1 Galerkin projection of random variable ψ onto the space of two polynomial chaos basis functions ϕ_1 and ϕ_2.

Table 1 Example of graded lexicographic ordering with $n_\xi = 3$.

$\lvert\boldsymbol{j}\rvert$	$\boldsymbol{j}$	j'
0	(0, 0, 0)	0
1	(1, 0, 0)	1
	(0, 1, 0)	2
	(0, 0, 1)	3
2	(2, 0, 0)	4
	(1, 1, 0)	5
	(1, 0, 1)	6
	(0, 2, 0)	7
	(0, 1, 1)	8
	(0, 0, 2)	9
3	(3, 0, 0)	10
	(2, 1, 1)	11
	$\vdots$	$\vdots$

D. Galerkin Projection of Stochastic Systems

As in [34], consider a random vector $\boldsymbol{s}^*(t, \boldsymbol{\xi})$ whose n_s components $s_i^*(t, \boldsymbol{\xi})$ are parametrized by $\boldsymbol{\xi}$ for $i \in \{1, \ldots, n_s\}$. These components can be approximated using gPCE as follows:

$$s_i^*(t, \boldsymbol{\xi}) \approx \tilde{s}_i(t, \boldsymbol{\xi}) := \sum_{|\boldsymbol{j}|=0}^{p} \underset{\sim}{s}_{i,\boldsymbol{j}}(t) \phi_{\boldsymbol{j}}(\boldsymbol{\xi}) \tag{34}$$

where $\underset{\sim}{s}$ are the gPC expansion coefficients. For compactness, we define

$$\tilde{\boldsymbol{s}}(t, \boldsymbol{\xi}) := \begin{bmatrix} \tilde{s}_1(t, \boldsymbol{\xi}) & \tilde{s}_2(t, \boldsymbol{\xi}) & \ldots & \tilde{s}_{n_s}(t, \boldsymbol{\xi}) \end{bmatrix}^{\mathsf{T}} \in \mathbb{R}^{n_s \times 1} \tag{35a}$$

If $\tilde{s}$ was the state vector for a dynamical system, for example, then $\tilde{s}_1, \ldots, \tilde{s}_{n_s}$ would be the individual components, and $\boldsymbol{s}^*(t,\boldsymbol{\xi}) \approx \tilde{\boldsymbol{s}}(t,\boldsymbol{\xi})$. Next we define

$$\underline{\boldsymbol{s}}_i(t) := \begin{bmatrix} \underline{s}_{i,0}(t) & \underline{s}_{i,1}(t) & \ldots & \underline{s}_{i,j'}(t) \end{bmatrix}^\mathsf{T} \in \mathbb{R}^{N_p \times 1} \tag{35b}$$

which is the column vector of N_p expansion coefficients for a given component of $\tilde{\boldsymbol{s}}$. Additionally, define

$$\boldsymbol{\phi}(\boldsymbol{\xi}) := \begin{bmatrix} \phi_0(\boldsymbol{\xi}) & \phi_1(\boldsymbol{\xi}) & \ldots & \phi_{j'}(\boldsymbol{\xi}) \end{bmatrix}^\mathsf{T} \in \mathbb{R}^{N_p \times 1} \tag{35c}$$

which is the column vector of N_p multivariate basis functions corresponding to each expansion coefficient. Lastly, we group the n_s column vectors $\underline{\boldsymbol{s}}_i$ to obtain

$$\boldsymbol{s}_{\text{PC}}(t) := \begin{bmatrix} \underline{\boldsymbol{s}}_1(t) & \ldots & \underline{\boldsymbol{s}}_{n_s}(t) \end{bmatrix} \in \mathbb{R}^{N_p \times n_s} \tag{35d}$$

We can now represent the gPCE as

$$\begin{aligned}
\tilde{\boldsymbol{s}}(t,\boldsymbol{\xi}) &= \boldsymbol{s}_{\text{PC}}^\mathsf{T}(t)\boldsymbol{\phi}(\boldsymbol{\xi}) && (36a)\\
&= \left(\boldsymbol{\phi}^\mathsf{T}(\boldsymbol{\xi}) \otimes \mathbb{I}_{n_s}\right) \text{vec}\left(\boldsymbol{s}_{\text{PC}}^\mathsf{T}(t)\right) && (36b)\\
&=: \Phi_s^\mathsf{T}(\boldsymbol{\xi})\boldsymbol{S}(t) && (36c)
\end{aligned}$$

where $\otimes$ is the Kroenecker product and vec$(\cdot)$ is the vectorization of a matrix [35]. Note that $\Phi_s^\mathsf{T}(\boldsymbol{\xi}) \in \mathbb{R}^{n_s \times n_s N_p}$ and $\boldsymbol{S}(t) \in \mathbb{R}^{n_s N_p \times 1}$.

E. Galerkin Projection of the Uncertain Augmented System

Substituting the gPCEs of $\boldsymbol{x}_A$, $\boldsymbol{y}_A$ and $\boldsymbol{z}$ into Eq. (28) we get

$$\begin{aligned}
\Phi_{x_A}^\mathsf{T}(\boldsymbol{\xi})\dot{\boldsymbol{X}}_A(t) &= \boldsymbol{A}_A(\boldsymbol{\xi})\Phi_{x_A}^\mathsf{T}(\boldsymbol{\xi})\boldsymbol{X}_A(t) + \boldsymbol{B}_A(\boldsymbol{\xi})\boldsymbol{u}(t) + \boldsymbol{G}\boldsymbol{\eta}(t) && (37a)\\
\Phi_{y_A}^\mathsf{T}(\boldsymbol{\xi})\boldsymbol{Y}_A(t) &= \boldsymbol{C}_A\Phi_{x_A}^\mathsf{T}(\boldsymbol{\xi})\boldsymbol{X}_A(t) + \boldsymbol{D}\boldsymbol{u}(t) + \boldsymbol{F}\boldsymbol{\eta}(t) && (37b)\\
\Phi_z^\mathsf{T}(\boldsymbol{\xi})\boldsymbol{Z}(t) &= \boldsymbol{L}\Phi_{x_A}^\mathsf{T}(\boldsymbol{\xi})\boldsymbol{X}_A(t) && (37c)
\end{aligned}$$

For brevity we will drop the $(\boldsymbol{\xi})$ notation from everything except $\boldsymbol{A}_A$ and $\boldsymbol{B}_A$. Now, multiply the dynamic equation by Φ_{x_A}, the measurement equation by Φ_{y_A}, and the estimate equation by Φ_z to get

$$\begin{aligned}
\Phi_{x_A}\Phi_{x_A}^\mathsf{T}\dot{\boldsymbol{X}}_A(t) &= \Phi_{x_A}\boldsymbol{A}_A(\boldsymbol{\xi})\Phi_{x_A}^\mathsf{T}\boldsymbol{X}_A(t) + \Phi_{x_A}(\boldsymbol{\xi})\boldsymbol{B}_A(\boldsymbol{\xi})\boldsymbol{u}(t) + \Phi_{x_A}\boldsymbol{G}\boldsymbol{\eta}(t) && (38a)\\
\Phi_{y_A}\Phi_{y_A}^\mathsf{T}\boldsymbol{Y}_A(t) &= \Phi_{y_A}\boldsymbol{C}_A\Phi_{x_A}^\mathsf{T}\boldsymbol{X}_A(t) + \Phi_{y_A}\boldsymbol{D}\boldsymbol{u}(t) + \Phi_{y_A}\boldsymbol{F}\boldsymbol{\eta}(t) && (38b)\\
\Phi_z\Phi_z^\mathsf{T}\boldsymbol{Z}(t) &= \Phi_z\boldsymbol{L}\Phi_{x_A}^\mathsf{T}\boldsymbol{X}_A(t) && (38c)
\end{aligned}$$

Now, take the expectation of Eq. (38) and let $\boldsymbol{M}_{x_A} = \mathbb{E}_\xi\left\{\Phi_{x_A}\Phi_{x_A}^\mathsf{T}\right\}$, $\boldsymbol{M}_{y_A} = \mathbb{E}_\xi\left\{\Phi_{y_A}\Phi_{y_A}^\mathsf{T}\right\}$ and let $\boldsymbol{M}_z = \mathbb{E}_\xi\left\{\Phi_z\Phi_z^\mathsf{T}\right\}$. By Eqs. (31) and (36), $\boldsymbol{M}_{x_A}$, $\boldsymbol{M}_{y_A}$ and $\boldsymbol{M}_z$ are diagonal and full rank. Thus,

$$\begin{aligned}
\boldsymbol{M}_{x_A}\dot{\boldsymbol{X}}_A(t) &= \mathcal{A}_A\boldsymbol{X}_A(t) + \mathcal{B}_A\boldsymbol{u}(t) + \mathcal{G}\boldsymbol{\eta}(t) && (39a)\\
\boldsymbol{M}_{y_A}\boldsymbol{Y}_A(t) &= \mathcal{C}_A\boldsymbol{X}_A(t) + \mathcal{D}\boldsymbol{u}(t) + \mathcal{F}\boldsymbol{\eta}(t) && (39b)\\
\boldsymbol{M}_z\boldsymbol{Z}(t) &= \mathcal{L}\boldsymbol{X}_A(t) && (39c)
\end{aligned}$$

where

$$\begin{aligned}
\mathcal{A}_A &= \mathbb{E}_\xi\left\{\Phi_{x_A}\boldsymbol{A}_A(\boldsymbol{\xi})\Phi_{x_A}^\mathsf{T}\right\} && \in \mathbb{R}^{n_x N_p \times n_x N_p} && (40a)\\
\mathcal{B}_A &= \mathbb{E}_\xi\left\{\Phi_{x_A}\boldsymbol{B}_A(\boldsymbol{\xi})\right\} && \in \mathbb{R}^{n_x N_p \times n_u} && (40b)\\
\mathcal{G} &= \mathbb{E}_\xi\left\{\Phi_{x_A}\boldsymbol{G}\right\} && \in \mathbb{R}^{n_x N_p \times n_\eta} && (40c)\\
\mathcal{C}_A &= \mathbb{E}_\xi\left\{\Phi_{y_A}\boldsymbol{C}_A\Phi_{x_A}^\mathsf{T}\right\} && \in \mathbb{R}^{n_y N_p \times n_x N_p} && (40d)\\
\mathcal{D} &= \mathbb{E}_\xi\left\{\Phi_{y_A}\boldsymbol{D}\right\} && \in \mathbb{R}^{n_y N_p \times n_u} && (40e)\\
\mathcal{F} &= \mathbb{E}_\xi\left\{\Phi_{y_A}\boldsymbol{F}\right\} && \in \mathbb{R}^{n_y N_p \times n_\eta} && (40f)\\
\mathcal{L} &= \mathbb{E}_\xi\left\{\Phi_z\boldsymbol{L}\Phi_{x_A}^\mathsf{T}\right\} && \in \mathbb{R}^{n_z N_p \times n_x N_p} && (40g)
\end{aligned}$$

Finally,

$$\dot{\boldsymbol{X}}_A(t) = \boldsymbol{M}_{x_A}^{-1}\Big(\mathcal{A}_A\boldsymbol{X}_A(t) + \mathcal{B}_A\boldsymbol{u}(t) + \mathcal{G}\boldsymbol{\eta}(t)\Big) \tag{41a}$$

$$\boldsymbol{Y}_A(t) = \boldsymbol{M}_{y_A}^{-1}\Big(\mathcal{C}_A\boldsymbol{X}_A(t) + \mathcal{D}\boldsymbol{u}(t) + \mathcal{F}\boldsymbol{\eta}(t)\Big) \tag{41b}$$

$$\boldsymbol{Z}(t) = \boldsymbol{M}_z^{-1}\mathcal{L}\boldsymbol{X}_A(t) \tag{41c}$$

From here we can abbreviate the notation once more and drop the (t). Note that, via gPCE, we have approximated the uncertain system, Eq. (28), as a deterministic system to which we can apply numerous well-established control and estimation tools.

IV. Steady-State gPC H_∞ Filter

In this section we design a deterministic state observer for the system (Eq. 39), which represents the original uncertain system (Eq. 28). Then we use H_∞ filter theory to obtain the static observer gain, resulting in augmented state estimates which have bounded error. Lastly, it is shown how the bound on the gPC system provides a bound on the uncertainty in the original system.

A. gPC H_∞ Filter Theory

A Luenberger filter for the system of Eq. (39) is of the form

$$\dot{\hat{\boldsymbol{X}}}_A = \mathcal{A}_A\hat{\boldsymbol{X}}_A + \mathcal{B}_A\boldsymbol{u} + \mathbb{K}\left(\boldsymbol{Y}_A - \mathcal{C}_A\hat{\boldsymbol{X}}_A\right) \tag{42}$$

$$\hat{\boldsymbol{Z}} = \mathcal{L}\hat{\boldsymbol{X}}_A \tag{43}$$

where the hat notation, $(\hat{\ })$, denotes an estimate, and $\mathbb{K}$ is a generic filter gain matrix to be determined. Now define $\tilde{\boldsymbol{X}}_A = \boldsymbol{X}_A - \hat{\boldsymbol{X}}_A$. Thus, the error dynamics of the filter are

$$\dot{\tilde{\boldsymbol{X}}}_A = (\mathcal{A}_A - \mathbb{K}\mathcal{C}_A)\,\tilde{\boldsymbol{X}}_A + (\mathcal{G} - \mathbb{K}\mathcal{F})\,\boldsymbol{\eta} \tag{44}$$

$$\tilde{\boldsymbol{Z}} = \boldsymbol{Z} - \hat{\boldsymbol{Z}} = \mathcal{L}\tilde{\boldsymbol{X}}_A \tag{45}$$

Define $L_2[0,\infty)$ as the space of square-integrable functions with bounded energy such that

$$\boldsymbol{\eta} \in L_2[0,\infty) \qquad \Rightarrow \qquad \int_0^\infty \|\boldsymbol{\eta}(t)\|_2^2 \mathrm{d}t < \infty \tag{46}$$

Let $\boldsymbol{H}_{\tilde{Z}\eta}(s)$ represent the transfer function from exogenous inputs, $\boldsymbol{\eta}$, to estimate error, $\tilde{\boldsymbol{Z}}$ for the system (44). Recall [36] that the H_∞ norm of system $\boldsymbol{H}_{\tilde{Z}\eta}(s)$ is given by

$$\|\boldsymbol{H}_{\tilde{Z}\eta}(s)\|_\infty = \operatorname*{ess\,sup}_{\omega_u\in\mathbb{R}} \sigma_{\max}\left(\boldsymbol{H}_{\tilde{Z}\eta}(j\omega_u)\right) = \sup_{\boldsymbol{0}\neq\boldsymbol{\eta}\in L_2} \frac{\|\tilde{\boldsymbol{Z}}\|_{L_2}}{\|\boldsymbol{\eta}\|_{L_2}} \tag{47}$$

where $\sigma_{\max}$ denotes the largest singular value, and $\|\cdot\|_{L_2}$ is the L_2-norm. From [11], we apply the following lemma:

Lemma 1 *(Adapted from Lemma 7.1(c) in [11]) For all $\boldsymbol{\eta} \in L_2[0,\infty)$, for a given $\gamma > 0$ there exists a linear causal filter such that $\boldsymbol{H}_{\tilde{Z}\eta}(s)$ is asymptotically stable and $\|\boldsymbol{H}_{\tilde{Z}\eta}(s)\|_\infty < \gamma$ if and only if the algebraic Riccati inequality (ARI)*

$$\mathcal{A}_A^\mathsf{T}\mathbb{X} + \mathbb{X}\mathcal{A}_A - \mathbb{Y}\mathcal{C}_A - \mathcal{C}_A^\mathsf{T}\mathbb{Y}^\mathsf{T} + \gamma^{-2}\mathcal{L}^\mathsf{T}\mathcal{L} + (\mathbb{X}\mathcal{G} - \mathbb{Y}\mathcal{F})(\mathbb{X}\mathcal{G} - \mathbb{Y}\mathcal{F})^\mathsf{T} < \boldsymbol{0} \tag{48}$$

has a solution $\mathbb{X} = \mathbb{X}^\mathsf{T} > \boldsymbol{0}$, with $\mathbb{Y} \in \mathbb{R}^{n\times m}$ where n is the number of states and m is the number of measurements. Applying the Schur complement to Eq. (48) yields the linear matrix inequality

$$\boldsymbol{\mathcal{Y}}(\mathbb{X},\mathbb{Y}) = \begin{bmatrix} \mathcal{A}_A^\mathsf{T}\mathbb{X} + \mathbb{X}\mathcal{A}_A - \mathbb{Y}\mathcal{C}_A - \mathcal{C}_A^\mathsf{T}\mathbb{Y}^\mathsf{T} + \gamma^{-2}\mathcal{L}^\mathsf{T}\mathcal{L} & \mathbb{X}\mathcal{G} - \mathbb{Y}\mathcal{F} \\ \mathcal{G}^\mathsf{T}\mathbb{X}^\mathsf{T} - \mathcal{F}^\mathsf{T}\mathbb{Y}^\mathsf{T} & -\boldsymbol{I} \end{bmatrix} < \boldsymbol{0} \tag{49a}$$

$$\mathbb{X} > \boldsymbol{0} \tag{49b}$$

Finally, the H_∞ filter gain, $\mathbb{K}_\infty$, is

$$\mathbb{K}_\infty = \mathbb{X}^{-1}\mathbb{Y} \tag{50}$$

B. Interpretation of H_∞ Results for gPC System

Recall from Eq. (36) that $\tilde{z} = \Phi_{\tilde{z}}^{\mathsf{T}}\tilde{\boldsymbol{Z}}$. Without loss of generality, let us normalize $\Phi_{\tilde{z}}$ such that $\langle\Phi_{\tilde{z}}, \Phi_{\tilde{z}}^{\mathsf{T}}\rangle$ is an identity matrix. Taking the expectation of $\|\tilde{z}\|_2^2$ we get

$$\mathbb{E}_\xi\{\|\tilde{z}\|_{L_2}^2\} = \mathbb{E}_\xi\left\{\int_0^\infty \tilde{z}^{\mathsf{T}}\tilde{z}\mathrm{d}t\right\} \tag{51a}$$

$$= \int_0^\infty \mathbb{E}_\xi\left\{\tilde{z}^{\mathsf{T}}\tilde{z}\right\}\mathrm{d}t \tag{51b}$$

$$= \int_0^\infty \tilde{\boldsymbol{Z}}^{\mathsf{T}}\mathbb{E}_\xi\{\Phi_{\tilde{z}}\Phi_{\tilde{z}}^{\mathsf{T}}\}\tilde{\boldsymbol{Z}}\mathrm{d}t \tag{51c}$$

$$= \|\tilde{\boldsymbol{Z}}\|_{L_2}^2 \tag{51d}$$

The above implies that, with $\mathbb{K}_\infty$ as the static filter gain,

$$\|\boldsymbol{H}_{\tilde{Z}\eta}(s)\|_\infty = \sup_{0\neq\eta\in L_2}\frac{\|\tilde{\boldsymbol{Z}}\|_{L_2}}{\|\boldsymbol{\eta}\|_{L_2}} = \sup_{0\neq\eta\in L_2}\frac{\sqrt{\mathbb{E}_\xi\{\|\tilde{z}\|_{L_2}^2\}}}{\|\boldsymbol{\eta}\|_{L_2}} < \gamma \tag{52}$$

From Eq. (52) we can see that by applying H_∞ filtering to the gPC expanded system we achieve a bound on the mapping from $\|\boldsymbol{\eta}\|_{L_2}$ to $\mathbb{E}_\xi\{\|\tilde{z}\|_{L_2}^2\}$. Thus, bounding the mapping from exogenous inputs to estimate error variance for the gPC system also bounds the corresponding mapping for the stochastic system.

V. Multivariate Uncertainty Reduction from Flight Test Data

A. Research Aircraft

The research aircraft used in this effort is the My Twin Dream (MTD), shown in Fig. 2, manufactured by My Fly Dream. It is a radio-controlled foam aircraft with counter-rotating twin electric motors and APC 10-in. diameter, 6-in. pitch (10x6) propellers. The aircraft was instrumented with a Cubepilot CubeOrange flight computer running PX4 firmware. The sensors onboard the aircraft include triple-redundant accelerometers and gyroscopes, two magnetometers, a Real-Time Kinematic (RTK) global positioning system (GPS) receiver, and a vaned air data unit for validation. The MTD was chosen for its simple construction, propeller location (to accommodate the air data boom), and endurance of approximately 25 minutes. The MTD's physical properties are listed in Table 2.

Fig. 2 My Twin Dream (MTD) aircraft

Table 2 My Twin Dream (MTD) properties

Property	Symbol	Value	Units
Mass	m	3.311	kg
Mean aerodynamic chord	$\bar{c}$	0.254	m
Projected wing span	b	1.800	m
Wing planform area	S	0.457	m^2
Roll moment of inertia	I_{xx}	0.319	kg-m^2
Pitch moment of inertia	I_{yy}	0.267	kg-m^2
Yaw moment of inertia	I_{zz}	0.471	kg-m^2
Product of inertia	I_{xz}	0.024	kg-m^2
Product of inertia	I_{xy}, I_{yz}	≈ 0	kg-m^2

The aerodynamic force and moment coefficients in Eq. (11) are from [20] and are reproduced in Table 5 in Appendix A along with their associated mean (μ), standard deviation (σ), and coefficient of variation (CV) [37]. The propulsion coefficient comes from a model based on the wind tunnel data from [21]. The accelerometers, gyroscopes, magnetometers, and GPS feed into an extended Kalman filter as part of the PX4 firmware, from which we use position ($\boldsymbol{X}$), attitude ($\boldsymbol{\Theta}$), and angular velocity (ω), which are provided along with their respective state estimate error variances [38]. The wind estimates were compared to reconstructed wind data from a vaned air data unit (ADU) mounted out the nose of the aircraft as pictured in Figure 2. This sensor was developed, manufactured, and calibrated by the Nonlinear Systems Laboratory at Virginia Tech [12]. It consists of two 3D printed vanes attached to magnetic rotary encoders and a 3D printed Kiel probe connected to a MS5525DSO[†] pressure sensor. The pulse-width modulation (PWM) rotary

[†]Manufactured by TE Connectivity

encoders are read at a sample rate of 200 Hz by a microcontroller that communicates with the flight computer over the CAN bus via a custom PX4 driver. The pressure sensor is natively supported by PX4 and configured to log calibrated airspeed data at 10 Hz.

Let V, α, and β_f be the airspeed, angle-of-attack, and flank angle reported by the ADU, respectively. By using GPS velocity measurements $\boldsymbol{v}_\mathrm{i}$ (accuracy of 0.05 m/s), autopilot attitude estimates (with quaternion estimate standard deviations $\approx 10^{-3}$), and angular velocity measurements from the calibrated gyroscope (noise and bias removed), the wind velocity may be reconstructed as

$$\boldsymbol{w} = \boldsymbol{v}_\mathrm{i} - \boldsymbol{R}_\mathrm{IB}\left(\boldsymbol{v}_\mathrm{ADU} - \boldsymbol{\omega} \times \boldsymbol{r}_\mathrm{ADU}\right) \tag{53}$$

where $\boldsymbol{v}_\mathrm{ADU} = \boldsymbol{R}_\mathrm{BW}(\alpha, \beta)\boldsymbol{e}_1 V_\mathrm{r}$. Here, $\boldsymbol{v}_\mathrm{ADU}$ is the air-relative velocity at the geometric center of the ADU vanes, whose position in the body frame is denoted $\boldsymbol{r}_\mathrm{ADU}$. The rotation matrix $\boldsymbol{R}_\mathrm{BW}(\alpha, \beta) = e^{-[\boldsymbol{e}_2\times]\alpha} e^{[\boldsymbol{e}_3\times]\beta}$, which maps free vectors from the wind frame to the body frame, is parameterized by the measured angle-of-attack, α, and the sideslip angle, $\beta = \tan^{-1}(\tan(\beta_f)\cos(\alpha))$. The accuracy of the reconstructed wind data can be characterized by propagating the measurement uncertainty through Eq. (53). Due to the low error of the constituent measurements, the reconstructed wind is treated as a truth source for wind estimate validation. This air data unit was validated in the Virginia Tech Aerospace and Ocean Engineering department's open jet wind tunnel both for steady-state readings and dynamic response. The airspeed-dependent cutoff frequencies of the vanes were found to be greater than 16 Hz, well above the fastest rigid body modes, which determine an upper limit on the dynamic response of model-based wind estimators.

B. Flight Test

A flight test campaign was conducted at Virginia Tech's Kentland Experimental Aerial Systems (KEAS) airfield on September 28th, 2022 using the UAS described in Section V.A. Data were gathered during four passes over the ground control station (referred to as Runs 1-4) at 76 m (250 ft) AGL when the wind conditions at ground level were gusty. Gusty conditions were chosen since the goal is to achieve accurate wind estimates under any condition in which the UAS is able to fly. Since we are utilizing an LTI model we restricted the maneuver to nominally steady flight, namely straight-and-level unaccelerated flight.

C. Computer Specifications

The simulations presented in this section were performed in Matlab R2023b on a laptop with an AMD Ryzen 7 PRO 7840U CPU with eight physical cores and 64 GB of DDR5-6400 memory. The MC simulations were accomplished using Matlab's `parfor` command[‡] and the gPC computations were accomplished analytically using symbolic integration along with `parfor`.

D. Methodology

This first step in computing the gPCE of Section III is to determine how the uncertainty in the nonlinear model parameters, given in Table 5 (Appendix A), maps to uncertainty in the entries of the linear system matrices. This is done analytically according to Section III.A. The resulting statistics for the $\boldsymbol{A}(\boldsymbol{\xi})$ matrix entries are presented in Table 3. Note that only the entries which are affected by changes in aerodynamic parameters, i.e. dynamic states and derivatives, are given. Next, a nominal filter (nom) is found using a deterministic method based on the nominal system, where $\boldsymbol{A}_\mathrm{nom} = \mathbb{E}_\xi\{\boldsymbol{A}(\boldsymbol{\xi})\}$. The H_∞ filtering method in [12] was used to produce the nominal filter $\left(H_\infty^\mathrm{nom}\right)$ results in this paper.

From Table 3 we identify the matrix entries we would like to analyze. Certainly there is no limit to the number of entries that can be included, but the computational burden of performing the gPCE grows according to N_p (Eq. (33)). This is commonly referred to as the *curse of dimensionality*. To simplify the results presented here we will only consider the three longitudinal entries with the largest CV from Table 3: $A_{7,7}$, $A_{9,7}$, and $A_{11,7}$. Since the distribution of each stochastic entry is Gaussian, the appropriate gPC polynomial basis is the family of Hermite polynomials [30], given by the formula

$$\mathrm{He}_n(\xi) = (-1)^n e^{\frac{\xi^2}{2}} \frac{\mathrm{d}^\mathrm{n}}{\mathrm{d}\xi^\mathrm{n}} e^{\frac{-\xi^2}{2}} \tag{54}$$

The first five Hermite polynomials are: $\mathrm{He}_0 = 1,\ \mathrm{He}_1 = \xi,\ \mathrm{He}_2 = \xi^2 - 1,\ \mathrm{He}_3 = \xi^3 - 3\xi,\ \mathrm{He}_4 = \xi^4 - 6\xi^2 + 3$. The corresponding probability density function is $\varphi(\xi) = \frac{1}{\sqrt{2\pi}} e^{-\frac{\xi^2}{2}}$ with support $\Omega = (-\infty, \infty)$. Recalling Section III.C, we

[‡]https://www.mathworks.com/products/parallel-computing.html

Table 3 Uncertain entries of linear A matrix

Axis of Motion	Deriv.(row)	State(col.)	Mean (μ)	Std. Dev. (σ)	CV $\left(\frac{\sigma}{\lvert\mu\rvert}\right)$
Longitudinal	$\dot{u}_r(7)$	$u_r(7)$	-0.197	0.090	0.46
	$\dot{w}_r(9)$	$u_r(7)$	-0.932	0.276	0.28
	$\dot{q}(11)$	$u_r(7)$	+0.015	0.066	4.12
		$w_r(9)$	-2.416	0.147	0.06
		$q(11)$	-9.684	0.233	0.02
Lateral-Directional	$\dot{v}_r(8)$	$v_r(8)$	-0.708	0.200	0.28
		$p(10)$	+0.474	0.207	0.44
		$r(12)$	-19.64	0.847	0.04
	$\dot{p}(10)$	$v_r(8)$	-0.997	0.133	0.13
		$p(10)$	-11.27	1.194	0.11
		$r(12)$	-0.177	0.043	0.24
	$\dot{r}(12)$	$v_r(8)$	+1.767	0.440	0.25
		$p(10)$	-0.574	0.061	0.10
		$r(12)$	-2.352	0.573	0.24

are not constrained to an assumption of normality to apply gPC. But, given the nature of the the uncertainties being considered, Gauss-Hermite polynomials are appropriate. Using the chosen uncertain entries of $\boldsymbol{A}(\boldsymbol{\xi})$, the gPC H_∞ filter $\left(H_\infty^{\text{gPC}}\right)$ is synthesized according to Section IV.A. The H_∞^{nom} and H_∞^{gPC} filters were used to generate wind estimates using available aircraft measurements: inertial position, Euler angles, and body angular rates. To characterize the uncertainty in wind estimates using the H_∞^{nom} filter Monte Carlo simulations were conducted, the details and results of which are presented in Part 1 [1]. Alternatively, the H_∞^{gPC} filter directly provides an estimate of the uncertainty (variance) as an output from a single run (See Section III.G of Part 1).

VI. Results

Figure 3 shows the MC simulations of the H_∞^{nom} filter with uncertainty in $A_{7,7}$, $A_{9,7}$, and $A_{11,7}$. The variation in the set of estimates $\{\hat{w}_N,\ \hat{w}_E,\ \hat{w}_D\}$ is purely a result of the uncertainty in the state matrix, $\boldsymbol{A}(\boldsymbol{\xi})$, which was ignored in the design of the H_∞^{nom} filter. In other words, $\boldsymbol{A}_{\text{nom}}$ was used to find $\boldsymbol{K}_\infty^{\text{nom}}$. Thus, the form of the filter equations used for the MC simulations [1] was

$$\dot{\hat{\boldsymbol{x}}}_A(t,\boldsymbol{\xi}) = \boldsymbol{A}_A(\boldsymbol{\xi})\hat{\boldsymbol{x}}_A(t,\boldsymbol{\xi}) + \boldsymbol{B}_A\boldsymbol{u}(t) + \boldsymbol{K}_\infty^{\text{nom}}\left(\boldsymbol{y}_A(t) - \boldsymbol{C}_A\hat{\boldsymbol{x}}_A(t,\boldsymbol{\xi})\right) \tag{55a}$$

$$\hat{z}(t,\boldsymbol{\xi}) = \boldsymbol{L}\hat{\boldsymbol{x}}_A(t,\boldsymbol{\xi}) \tag{55b}$$

Since for this particular test case the aircraft was flown on a north-south course (see Figure 4) we would expect the longitudinal uncertainty to manifest as uncertainty in the north wind component. As can be seen in Figure 3, the north component, $\hat{w}_N$, is affected the most by these uncertainties (i.e., it has the largest variance in estimates over time), followed by the east component, $\hat{w}_E$. The downward component, $\hat{w}_D$, is much less affected. For reference the actual wind values $(w_N,\ w_E,\ w_D)$ measured by the ADU discussed in Section V.A are also shown.

Again, our goal is to leverage knowledge of $\boldsymbol{A}(\boldsymbol{\xi})$ to reduce the variance (i.e., improve the precision) of the wind estimates given in Figure 3. In Part 1 [1] it was found that, for this particular system, a 2nd order gPCE was sufficient for accurately characterizing the underlying uncertainty. Thus, $p = 2$ was chosen for synthesizing the H_∞^{gPC} filter according to Section IV. Table 4 presents the variance in the wind estimates for the H_∞^{nom} and H_∞^{gPC} filters. Maximum (Max), root-mean-squared (RMS), and average (Avg.) variances are given, as well as the percent reduction, $\%\Delta$, from the nominal filter to the gPC-based filter. The H_∞^{gPC} filter is able to achieve significant reductions in variance across all three metrics.

Figure 5 shows that H_∞^{gPC} filter is able to track the mean wind value similar to the H_∞^{nom} filter. Figures 6-8 show the variance in the estimates over time and how the H_∞^{gPC} filter is effective at generating estimates that are closer to the mean and, therefore, is less sensitive to uncertainty in the underlying model. Thus, the H_∞^{gPC} filter is able to reduce potential wind estimate error due to imprecisely known model parameters.

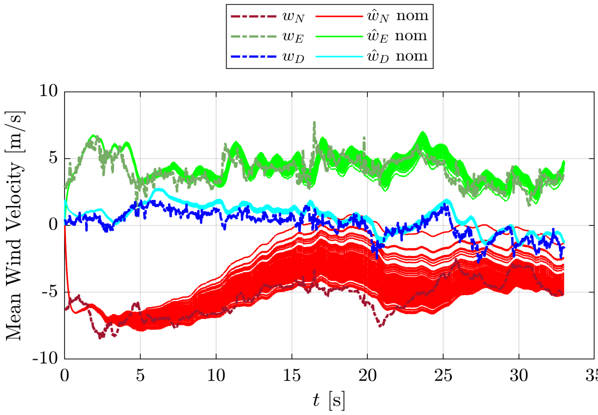

Fig. 3 Monte Carlo simulations of the nominal filter with uncertainty in the longitudinal entries of $A(\xi)$.

Fig. 4 Test flight path (results data segment outlined in black).

Table 4 Variance in wind estimates for nominal and 2nd order gPC H_∞ filters with $n_\xi = 3,\ (A_{7,7}, A_{9,7}, A_{11,7})$

		Variance					
Filter Method	Wind Component	Max	%Δ from nom	RMS	%Δ from nom	Avg.	%Δ from nom
H_∞^{nom}	w_N	0.763	–	0.451	–	0.374	–
	w_E	0.056	–	0.033	–	0.027	–
	w_D	0.006	–	0.004	–	0.003	–
H_∞^{gPC}	w_N	0.672	11.9	0.346	23.2	0.282	24.5
	w_E	0.049	11.9	0.025	23.2	0.021	24.5
	w_D	0.006	0.9	0.003	16.4	0.003	16.2

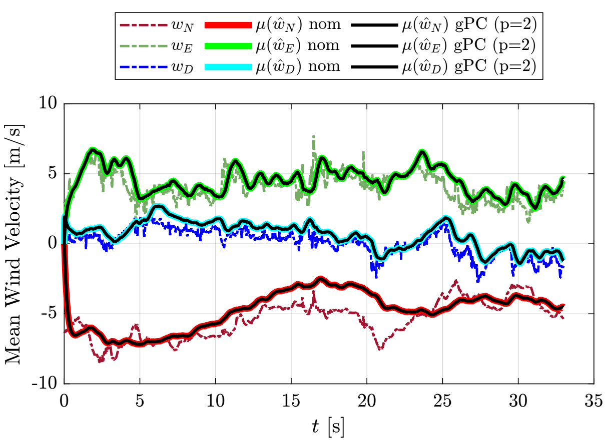

Fig. 5 Mean wind velocities from MC of H_∞^{nom} filter and single run of H_∞^{gPC} filter.

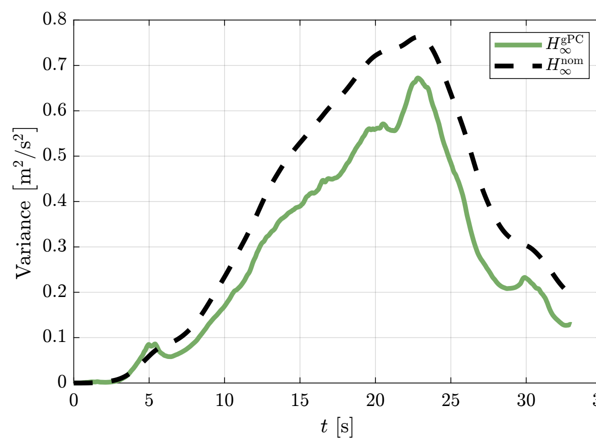

Fig. 6 Variance in $\hat{w}_N$ calculated from MC of H_∞^{nom} filter and single run of H_∞^{gPC} filter.

VII. Conclusions and Comments

This paper describes the underlying theory and process for obtaining a deterministic system of equations from a stochastic system using gPC. The concepts are applied to the problem of model-based wind estimation using measurements obtained from an unmanned aircraft. The aim is to obtain a measure of the precision of these wind estimates over time, given known uncertainties in model parameters. Additionally, we seek to use knowledge of the uncertainties to improve the precision of the wind estimates. In the multivariate case presented here the H_∞^{gPC} filter shows superiority over the nominal H_∞ filter in terms of variance in estimates due to model parametric uncertainty. It has been shown that the error due to parametric uncertainty, as characterized by the variance in estimates from the mean,

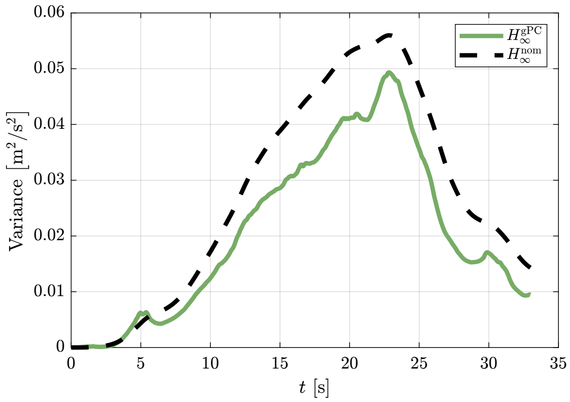

Fig. 7 Variance in $\hat{w}_E$ calculated from MC of H_∞^{nom} filter and single run of H_∞^{gPC} filter.

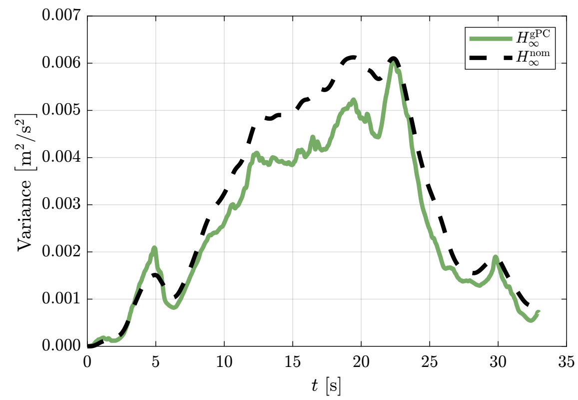

Fig. 8 Variance in $\hat{w}_D$ calculated from MC of H_∞^{nom} filter and single run of H_∞^{gPC} filter.

is reduced by almost 25% on average by using a 2nd order gPCE. These results can likely be improved by adjusting weightings within the H_∞ formulation or restructuring the gPCE system and is an area of future research. Additionally, in practice the H_∞^{gPC} filter could be used in applications, such as in a synthetic air data system, to obtain estimates and their associated uncertainty in real-time. This is not possible using MC. The methods presented here are extensible to nonlinear systems [25] and interdependent uncertainties [39, 40], so the applications are manifold. Together, Part 1 [1] and this work demonstrate the utility and versatility of gPC for wind and state estimation.

Appendix A. Nonlinear Model Parameters

Table 5 Nonlinear Model Parameters [20]

Axis of Motion	Coefficient	Parameter	Mean (μ)	Std. Dev. (σ)	CV $\left(\frac{\sigma}{\lvert\mu\rvert}\right)$
Longitudinal	C_X	C_{X_0}	+0.009	0.026	2.89
		C_{X_α}	+0.282	0.000	0.00
		$C_{X_{\alpha^2}}$	+3.173	0.119	0.04
		$C_{X_{\delta_e}}$	+0.051	0.025	0.49
	C_Z	C_{Z_0}	-0.255	0.074	0.29
		C_{Z_α}	-4.436	0.015	0.00
		C_{Z_q}	-12.54	0.030	0.00
	C_m	C_{m_0}	+0.008	0.006	0.75
		C_{m_α}	-0.444	0.027	0.06
		C_{m_q}	-14.02	0.336	0.02
		$C_{m_{\delta_e}}$	-0.415	0.058	0.14
Lateral-Directional	C_Y	C_{Y_β}	-0.410	0.115	0.28
		C_{Y_p}	+0.221	0.133	0.60
		C_{Y_r}	+0.230	0.547	2.38
		$C_{Y_{\delta_a}}$	+0.118	0.011	0.09
		$C_{Y_{\delta_r}}$	+0.136	0.030	0.22
	C_l	C_{l_β}	-0.035	0.004	0.11
		C_{l_p}	-0.386	0.041	0.11
		$C_{l_{\delta_a}}$	-0.137	0.010	0.07
	C_n	C_{n_β}	+0.083	0.020	0.24
		C_{n_r}	-0.119	0.029	0.24
		$C_{n_{\delta_a}}$	+0.013	0.009	0.69
		$C_{n_{\delta_r}}$	-0.068	0.006	0.09

Acknowledgements

The authors would like to thank Mekonen H. Halefom[§] for his support during flight test activities. The authors also gratefully acknowledge the sponsorship of NASA under Grant No. 80NSSC20M0162 as well as the support of the U.S. Air Force and Virginia Tech's Kevin T. Crofton Department of Aerospace and Ocean Engineering.

References

[1] Gahan, K. C., Hopwood, J. W., and Woolsey, C. A., "Uncertainty in Wind Estimates, Part 1: Analysis using Generalized Polynomial Chaos," *AIAA SCITECH 2024 Forum*, Orlando, FL, 2024. To Appear.

[2] González-Rocha, J., De Wekker, S. F. J., Ross, S. D., and Woolsey, C. A., "Wind Profiling in the Lower Atmosphere from Wind-Induced Perturbations to Multirotor UAS," *Sensors*, Vol. 20, No. 5, 2020. https://doi.org/10.3390/s20051341.

[3] Fuhrmann, M., and Horowitz, M. C., "Droning on: Explaining the Proliferation of Unmanned Aerial Vehicles," *International Organization*, Vol. 71, No. 2, 2017, pp. 397–418. https://doi.org/10.1017/S0020818317000121.

[4] National Oceanic and Atmospheric Administration, Dept. of Defense, Federal Aviation Administration, and the United States Navy, "Automated Surface Observing Systems (ASOS) User's Guide," , Mar 1998.

[5] Lie, F., and Gebre-Egziabher, D., "Synthetic Air Data System," *Journal of Aircraft*, Vol. 50, 2013, pp. 1234–1249. https://doi.org/10.2514/1.C032177.

[6] Lee, J. H., Sevil, H., Dogan, A., and Hullender, D., "Estimation of Maneuvering Aircraft States and Time-Varying Wind with Turbulence," *AIAA Guidance, Navigation, and Control Conference*, Minneapolis, MN, 2012. https://doi.org/10.2514/6.2012-4532.

[7] Ahmed, Z., Halefom, M. H., and Woolsey, C. A., "A Survey of Wind Estimation Methods using Small Uncrewed Aerial Vehicles," *(In review.)*, 2023.

[8] Mcmanus, H. L., and Hastings, D. E., "A Framework for Understanding Uncertainty and its Mitigation and Exploitation in Complex Systems," *IEEE Engineering Management Review*, Vol. 34, No. 3, 2006, pp. 81–81. https://doi.org/10.1109/EMR.2006.261384.

[9] Danowsky, B. P., Chrstos, J. R., Klyde, D. H., Farhat, C., and Brenner, M., "Evaluation of Aeroelastic Uncertainty Analysis Methods," *Journal of Aircraft*, Vol. 47, No. 4, 2010, pp. 1266–1273. https://doi.org/10.2514/1.47118.

[10] Kiureghian, A. D., and Ditlevsen, O., "Aleatory or epistemic? Does it matter?" *Structural Safety*, Vol. 31, No. 2, 2009, pp. 105–112. https://doi.org/10.1016/j.strusafe.2008.06.020.

[11] Lewis, F., Xie, L., and Popa, D., *Optimal and Robust Estimation with an Introduction to Stochastic Control Theory*, 2nd ed., Taylor & Francis Group, LLC., Boca Raton, FL, 2008, Chaps. 2,8.

[12] Gahan, K. C., Hopwood, J. W., and Woolsey, C. A., "Wind Estimation using an H_∞ Filter with Fixed-Wing Aircraft Flight Test Results," *AIAA SCITECH 2023 Forum*, National Harbor, MD, 2023. https://doi.org/10.2514/6.2023-2252.

[13] Xiu, D., and Karniadakis, G. E., "Modeling uncertainty in flow simulations via generalized polynomial chaos," *Journal of Computational Physics*, Vol. 187, No. 1, 2003, pp. 137–167. https://doi.org/10.1016/S0021-9991(03)00092-5.

[14] Stull, R., "Mean Boundary Layer Characteristics," *An Introduction to Boundary Layer Meteorology*, Kluwer Academic Publishers, Dordrecht, The Netherlands, 1988, pp. 5–6. https://doi.org/10.1007/978-94-009-3027-8.

[15] González-Rocha, J., Woolsey, C. A., Sultan, C., and De Wekker, S. F. J., "Sensing Wind from Quadrotor Motion," *Journal of Guidance, Control, and Dynamics*, Vol. 42, No. 4, 2019, pp. 836–852. https://doi.org/10.2514/1.G003542.

[16] Kundu, P. K., and Cohen, I. M., *Fluid Mechanics*, 3rd ed., Elsevier Academic Press, 2004.

[17] Etkin, B., "General Equations of Unsteady Motion," *Dynamics of Atmospheric Flight*, John Wiley and Sons, New York, 1972, pp. 121–157.

[18] Frost, W., and Bowles, R. L., "Wind Shear Terms in the Equations of Aircraft Motion," *Journal of Aircraft*, Vol. 21, No. 11, 1984, pp. 866–872. https://doi.org/10.2514/3.45056.

[§]PhD Candidate, Kevin T. Crofton Department of Aerospace and Ocean techniques Engineering, AIAA Student Member

[19] McClelland, H. G., and Woolsey, C. A., "Effects of Two Modeling Assumptions on Wind Reconstruction from Longitudinal Aircraft Motion," *Journal of Guidance, Control, and Dynamics*, Vol. 43, No. 6, 2020, pp. 1069–1081. https://doi.org/10.2514/1.G004224.

[20] Halefom, M. H., Gresham, J. L., and Woolsey, C. A., "Modeling and System Identification of Unsteady Aerodynamic Parameters for a Small Fixed-wing Aircraft," *(In preparation.)*, 2023.

[21] Brandt, J., Deters, R., Ananda, G., Dantsker, O., and Selig, M., "UIUC Propeller Database,Vols 1-4," , Nov 2022. Retrieved from https://m-selig.ae.illinois.edu/props/propDB.html.

[22] Yechout, T. R., "Aircraft Equations of Motion," *Introduction to Aircraft Flight Mechanics*, AIAA Education Series, American Institute of Aeronautics & Astronautics, Reston, VA, 2014, 2^{nd} ed., pp. 163–192. https://doi.org/10.2514/4.102547.

[23] Gahan, K. C., Hopwood, J. W., and Woolsey, C. A., "Wind Estimation using an H_∞ Filter with Fixed-Wing Aircraft Flight Test Results," *(In review.)*, 2023.

[24] Morelli, E. A., and Klein, V., *Aircraft System Identification: Theory and Practice*, 2^{nd} ed., Sunflyte Enterprises, Williamsburg, VA, 2016. ISBN:978-0-9974306-1-5.

[25] de Freitas Virgilio Pereira, M., "Polynomial Chaos-based Control Design for an Aircraft at High Angles of Attack with Uncertain Aerodynamics," Ph.D. thesis, Instituto Tecnologico de Aeronautica, 2017.

[26] Xu, Y., "Uncertainty Quantification, State, and Parameter Estimation in Power Systems using Polynomial Chaos Based Methods," Ph.D. thesis, Virginia Polytechnic Institute and State University, 2020.

[27] Walters, G., "Application of Generalized Polynomial Chaos to Flow-Induced Vibration and Sound," Ph.D. thesis, The Pennsylvania State University, 2020.

[28] Lemons, D. S., *An Introduction to Stochastic Processess in Physics*, Springer Finance Textbooks, Johns Hopkins University Press, 2002. ISBN:0-8018-6866-1.

[29] Cox, D., Little, J., and O'Shea, D., *Ideals, Varieties, and Algorithms: An Introduction to Computational Algebraic Geometry and Commutative Algebra*, 4^{th} ed., Springer Int'l Publishing, Switzerland, 2015, Chap. 2. https://doi.org/10.1007/978-3-319-16721-3.

[30] Xiu, D., "Generalized Polynomial Chaos," *Numerical Methods for Stochastic Computations: A Spectral Method Approach*, Princeton University Press, 2010, pp. 57–67. https://doi.org/10.5555/1893088.

[31] Xiu, D., and Karniadakis, G. E., "The Wiener–Askey Polynomial Chaos for Stochastic Differential Equations," *SIAM Journal on Scientific Computing*, Vol. 24, No. 2, 2002, p. 619–644. https://doi.org/10.1137/s1064827501387826.

[32] Cameron, R. H., and Martin, W. T., "The Orthogonal Development of Non-linear Functionals in Series of Fourier-Hermite Functionals," *The Annals of Mathematics*, Vol. 48, No. 2, 1947, p. 385. https://doi.org/10.2307/1969178.

[33] Debusschere, B., "Intrusive Polynomial Chaos Methods for Forward Uncertainty Propogation," *Handbook of Uncertainty Quantification*, edited by R. Ghanem, D. Higdon, and H. Owhadi, Springer Int'l Publishing, Switzerland, 2017, Chap. 17, pp. 617–636. https://doi.org/10.1007/978-3-319-11259-6.

[34] Wan, Y., Shen, D. E., Lucia, S., Findeisen, R., and Braatz, R. D., "Robust static $\mathcal{H}_\infty$ output-feedback control using Polynomial Chaos," *2018 Annual American Control Conference (ACC)*, Milwaukee, WI, 2018. https://doi.org/10.23919/acc.2018.8431074.

[35] Horn, R. A., and Johnson, C. R., *Matrix Analysis*, Cambridge University Press, 1985. https://doi.org/10.1017/CBO9780511810817.

[36] Dullerud, G. E., and Paganini, F., *A Course in Robust Control Theory: A Convex Approach*, 2000.

[37] Everitt, B., and Skrondal, A., *The Cambridge Dictionary of Statistics*, Cambridge University Press, 2010. https://doi.org/10.1111/j.1751-5823.2011.00149_2.x.

[38] Riseborough, P., "Using the ECL EKF," , Accessed Nov 2022. Retrieved from https://docs.px4.io/main/en/advanced_config.html.

[39] Navarro, M., Witteveen, J., and Blom, J., "Polynomial Chaos Expansion for general multivariate distributions with correlated variables," *arXiv*, 2014. https://doi.org/10.48550/arXiv.1406.5483.

[40] Rahman, S., "A Polynomial Chaos Expansion in Dependent Random Variables," *Journal of Mathematical Analysis and Applications*, Vol. 464, No. 1, 2018, pp. 749–775. https://doi.org/10.1016/j.jmaa.2018.04.032.